Journal of Nuclear Materials 390–391 (2009) 1110–1113

Contents lists available at ScienceDirect

Journal of Nuclear Materials

journal homepage: www.elsevier.com/locate/jnucmat

A sodium (Na) beam edge diagnostic

E. Wolfrum [a,*], J. Schweinzer [a], D. Bridi [b], K. Igenbergs [b], J. Kamleitner [b], F. Aumayr [b], ASDEX Upgrade Team

[a] Max Planck Institut für Plasmaphysik, EURATOM Association, Boltzmannstrasse 2, D-85748 Garching, Germany
[b] Institut für Allgemeine Physik, TU Wien, EURATOM Association ÖAW, Wiedner Hauptstr. 8-10/134, A-1040 Wien, Austria

A B S T R A C T

A fast (40–80 keV) neutral sodium (Na) beam is considered as advantageous alternative to the fast lithium (Li) beam installed at ASDEX Upgrade. Recently, a complete data set of all relevant plasma particles (electron, ions) – Na collisions has been compiled [1] and first experiments with a Na beam installed at ASDEX Upgrade have been carried out. A collisional radiative model is employed to calculate the beam attenuation in a plasma discharge as well as the occupation number of Na excited states (including $n = 3, 4, 5s$). Excellent agreement between modeled and measured Na I emission profiles is found, proving the validity of the compiled data set. Despite the lower velocity at the same acceleration voltage, beam penetration of Na as compared with Li is not significantly deteriorated. The influence of electron temperature (T_e) and Z_{eff} profiles on evaluated electron density (n_e) profiles is analyzed.

1. Introduction

Steep density and temperature gradients characterize the edge plasma of tokamaks in the H-mode (high confinement mode). Within a few centimeters n_e rises one order of magnitude, T_e can even increase by two orders of magnitude. At ASDEX Upgrade the measurements in this region are provided by a number of different diagnostics, which are located at different places around the torus [2].

The 40–50 keV lithium beam diagnostic at ASDEX Upgrade [3–5] delivers routinely n_e profiles and for selected discharges T_i and n_i profiles. A novel probabilistic evaluation algorithm involving Bayesian statistics [6] allows the determination of the pedestal top densities up to n_e of 7×10^{19} m^{-3}. In order to improve this diagnostic further the lithium emitter can be replaced by a sodium (Na) emitter. There are several advantages of a Na emitter when compared to Li: (i) the emitter temperature can be kept lower, thus improving the withstand voltage and the stability of the ion source at higher voltages (>60 kV), (ii) the charge exchange cross sections for collisions with relevant impurity ions (He, C) are larger, facilitating ion temperature measurements, (iii) the lifetime of the observed transition (Na I (3p–3s)) is with 16.2 ns shorter than the Li I (2p–2s) with 26.9 ns, which is of benefit to the planned density fluctuation measurements [7], (iv) the neutralization of the ion beam occurs in a Na cell. As the charge exchange cross section between Na^+ and Na^0 is higher than between Li^+ and Na^0, a high neutralization efficiency is achieved at lower densities in the charge exchange cell and (v) the observed transition (Na I (3p–3s)) emits photons at a wavelength of 588.9 nm. The used photomultipliers have a higher sensitivity in the yellow region than in the red (Li I @ 670.8 nm), leading again to a signal-to-noise ratio improvement.

The only disadvantages of Na when compared to Li are the higher atomic mass and the slightly smaller ionization energy, raising the question whether Na atoms will penetrate as far as Li into the plasma and provide n_e data at the pedestal top.

2. Modeling

The beam attenuation modeling takes into account all collisions of the neutral beam atoms with plasma particles, including electron and proton impact excitation, ionization and charge exchange processes. The spatial occupation number densities N_i of atomic states i (Li: 10 states: 2s, 2p, ..., 4f and Li^+; Na: 9 states: 3s, 3p, ..., 5s and Na^+) are described by a system of coupled linear differential equations:

$$\frac{dN_i(Z)}{dZ} = \sum_{j=1}^{N} \{n_e(Z) a_{ij}(T_e(Z)) + b_{ij}\} N_j(Z), \quad (1)$$

z is the coordinate along the injected lithium beam, the coefficients a_{ij} contain the population and depopulation rate coefficients from level i-> j due to collisions with electrons, protons and impurity ions, the coefficients b_{ij} are the Einstein coefficients for the radiative transitions.

The rate coefficients a_{ij} are calculated using the database described in [1], where all relevant cross sections are given in the form of a recommended fit to theoretical as well as experimental data. Below a beam energy of 20 keV the fits are not valid any longer, because the relative collision velocities become too small.

* Corresponding author.
E-mail addresses: e.wolfrum@ipp.mpg.de (E. Wolfrum), aumayr@iap.tuwien.ac.at (F. Aumayr).

0022-3115/$ - see front matter © 2009 Elsevier B.V. All rights reserved.
doi:10.1016/j.jnucmat.2009.01.282

In the following we will show modeled Na I emission profiles for four density profiles with varying pedestal top density values. We chose single time spans out of typical discharge scenarios, such as the standard ohmic and the standard H-mode shot of ASDEX Upgrade, as well as two discharges where both, the Na I and the Li I emission profile could be measured (see sections 3 and 4).

In Fig. 1 the n_e (1a) and T_e (1b) profiles for the four different discharges are plotted. The data shown are fits to experimentally determined values (density: lithium beam diagnostic and edge Thomson scattering diagnostic, temperature: ECE diagnostic and edge Thomson scattering diagnostic) mapped to the magnetic midplane. For details of n_e and T_e pedestal top values as well as position of the separatrix see Table 1.

Fig. 2 displays the modeled emission profiles: (2a) for a Li beam at 40 keV and (2b) for a Na beam at 40 and 80 keV. The profiles shown in Fig. 1 are used as input for modeling.

The most striking observation is that the maxima of the Na I emission profiles are only slightly shifted to the outside. Also, the difference between a 40 and 80 keV Na beam is only marginal. This is mainly due to the fact that the excited states of Na are considerably less occupied than in the case of Li and consequently the very efficient charge exchange from these states, contributing to the attenuation of the beam, plays a minor role. The penetration depth of a Na beam is thus only slightly shorter than a Li beam at an acceleration voltage of 40 keV. For higher acceleration voltages, the penetration depth of Li increases considerably, while the one of Na hardly changes.

The evaluation of n_e relies on the inversion of the second equation of (Eq. (1)) applying a shooting method [8] and is numerically very sensitive to a singularity condition at a certain z value ($\sum_j a_{2j} N_j = 0$, i.e. population equals depopulation of the Li(2p)/Na(3p) state by collisions). Due to less populated excited states in the case of Na, the position of the singularity is shifted to larger z with respect to the maximum of the emission profile. Table 1 also lists the penetration depths, i.e. where the ground state is attenuated to 5%, and the positions of the singularity for the case of 40 keV Li and 40 and 80 keV Na beams for the four chosen discharge scenarios. While the Li beam penetrates deeper into the plasma, the position of the singularity and thus the point up to which an evaluation of n_e is possible is similar for both species.

A detailed comparison of electron densities and their uncertainties derived from the novel probabilistic evaluation algorithm [6], where the singularity is irrelevant, is part of future work.

2.1. Temperature dependence

During routine plasma operation T_e profiles are not immediately available. Therefore a typical T_e profile is taken as input for n_e evaluation. Such a profile is described by a tanh-shaped curve typical for the edge transport barrier (ETB) zone. At the separatrix position T_e is set to 100 eV [9]. T_e values in the SOL are usually not well determined and can range from 5 to 20 eV. The width of the pedestal, i.e. the width of the tanh-shaped curve from the top to the bottom values changes with discharge type (L-mode, H-mode) as well as with heating power. The dependence of the evaluated n_e profiles on the uncertainty in the assumed T_e was tested in two separate steps: (i) the profile shape was kept constant for $\rho_{pol} < 1$ and for $\rho_{pol} > 1$ the SOL temperatures (T_e^{SOL}) were set to fixed values of 2, 5, 10, 20 and 50 eV (see Fig. 3(a)). The reconstructed n_e did not show any effect of these T_e^{SOL} changes for $\rho_{pol} < 1$ (as shown in Fig. 3(b)). For $\rho_{pol} > 1$ the most significant difference occurred for a T_e^{SOL} of 2 eV, which is below the excitation threshold of the 3p–3s transition. For all other settings the calculated n_e profiles did not differ by more than 25% (see Fig. 3(c), where the quotient to

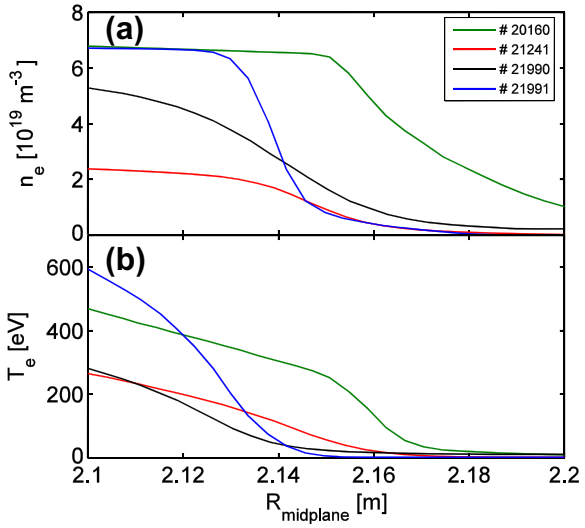

Fig. 1. (a) n_e and (b) T_e profiles for discharges #20160 (green), #21241 (red), #21990 (black), #21991 (blue) vs. midplane radius.

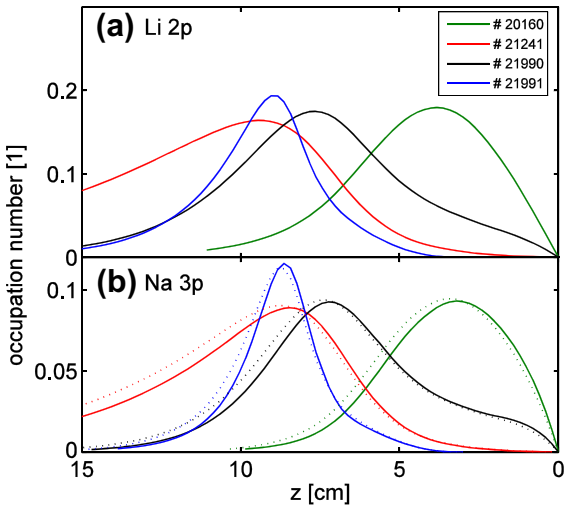

Fig. 2. (a) Li 2p (E_{beam} = 40 keV) and (b) Na 3p (E_{beam} = 40 keV, E_{beam} = 80 keV dotted) occupation profiles vs. beam coordinate modeled for n_e and T_e profiles of Fig. 1.

Table 1
For the selected n_e profiles: shot number (#), pedestal top electron density (n_e^{ped}) and temperature (T_e^{ped}), position of the separatrix (R_{sep}), for 40 keV Li and 40 keV as well as 80 keV Na: penetration depth (ρ) and point of singularity (sing.) in normalized poloidal radius (ρ_{pol}).

#	n_e^{ped} = 0.95 10^{19} m^{-3}	T_e^{ped} = 0.95 eV	R_{sep} m	$\rho^{Li}_{40\ kV}$ ρ_{pol}	Sing. ρ_{pol}	$\rho^{Na}_{40\ kV}$ ρ_{pol}	sing. ρ_{pol}	$\rho^{Na}_{80\ kV}$ ρ_{pol}	Sing. ρ_{pol}
20160	6.59	400	2.156	0.95	1.00	0.97	0.97	0.96	0.98
21241	2.24	220	2.145	0.80	–	0.85	–	0.83	–
21990	5.16	280	2.138	0.92	0.99	0.95	–	0.94	0.96
21991	6.70	550	2.14	0.94	0.99	0.96	0.98	0.95	0.99

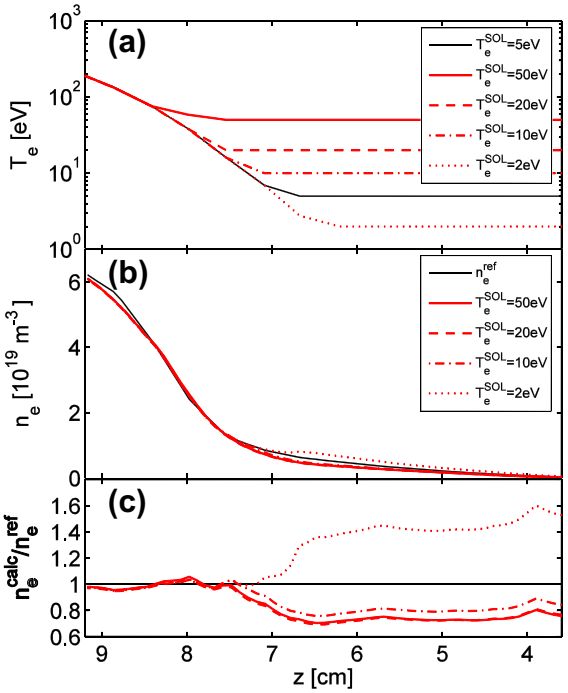

Fig. 3. #21 991: (a) T_e profile, varying T_e^{SOL}, (b) n_e^{calc} compared to n_e^{ref} (black), (c) ratio to n_e^{ref}.

the reference profile is shown). (ii) The width of the Te profiles was varied between 10 and 80 mm while keeping T_e^{SOL} = 5 eV, T_e^{sep} = 100 eV and T_e^{ped} = 800 eV. Also here the reconstructed n_e were not affected significantly. As the evaluated n_e profiles are not sensitive to the chosen T_e profile, two typical T_e profiles were selected, one for H-mode and one for L-mode plasmas. The appropriate profile is selected by a regime identification algorithm and subsequently used for n_e determination.

2.2. Z_{eff} dependence

So far modeling was presented for clean D plasmas. Reduced excitation and ionization rates $\langle\sigma v\rangle/v_{beam}$, where < . > denotes averaging over the Maxwell distribution, for collisions of Na with plasma electrons and protons were used.

Due to the heavier mass of impurity ions, the collision velocity can be approximated by the Na beam energy. The reduced rates $\langle\sigma v\rangle/v_{beam}$ are simply replaced by the cross sections $\sigma(v_{beam})$, which are easily derived from cross sections for Na atoms colliding with protons and He^{2+} via scaling relations [1].

The density of impurity ions can be described by only two parameters, Z_{eff} and q, that can vary for different ρ_{pol}. q is the mean charge of the impurity ions and the effective charge Z_{eff} is defined as $Z_{eff} := (n_p + n_i q^2)/n_e$, where n_i denotes the ion density.

Out of both values the fraction of ions with respect to electrons in the plasma is calculated (frac $\cdot\, q = Z_{eff} - 1/q - 1$). A pure helium plasma corresponds to Z_{eff} = 2, q = 2, the fraction becomes 0.5.

Fig. 4 shows, that Na I emission for a helium plasma is lower than for D plasma. The backward calculated n_e-profiles are the same.

Fig. 4 also shows what happens, if a false Z_{eff} profile is used. If the calculation is done for He plasma, but the emission profile is measured in a D plasma, the calculated n_e is too low. If the calculation is done for D plasma, but the emission profile is measured in a He plasma, the inverted effect occurs, the calculated n_e is too high. For these completely false Z_{eff} profiles the differences in n_e are about 15%, and for reasonably realistic Z_{eff} profiles these errors remain below 5%.

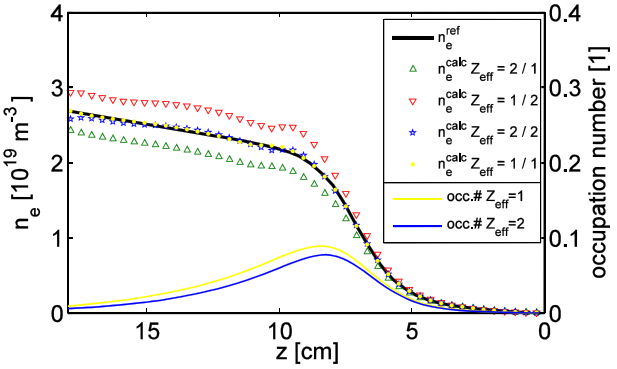

Fig. 4. #21 241: left axis: n_e^{ref} (black) compared to reconstructed n_e profiles: the first index gives the species for the modeled Na 3p profile, the second for the assumption of the reconstruction: D/D (yellow dots), He/He (blue stars), D/He (red triangles), He/D (green triangles); right axis: Na 3p occupation number for D (yellow line) and He (blue line).

3. Experiment

In order to test the viability of a Na beam for n_e measurements without compromising the routine operation of the Li beam, a combined Na/Li emitter was produced. To the β-eucryptite powder ($LiAlSiO_4$), which is normally used for our Li emitters, $NaAlSiO_4$ was added in a ratio Li:Na = 9:1. The powder was applied on top of the heating element and slowly heated to ~1300 °C, resulting in a ceramic surface after cooling. Ten such layers were applied consecutively.

The experimental setup of the Lithium beam diagnostic at ASDEX Upgrade is shown in [5, Fig. 1]. The optical head at the top of the vessel is equipped with 35 optical fibers, guiding the light to filter-photomultiplier detectors, where the Li I emission is recorded. Another optical head at the bottom is equipped with two rows of 30 fibers each, guiding the light to a switch board, where 18 lines of sight can be selected and analyzed with two Czerny Turner spectrometers, both connected to frame transfer CCD cameras. The spectra are recorded with a frame rate of 4 ms.

The acceleration voltage for the Li/Na emitter was set to 40 keV. The beam optics does not contain any mass separation, so both species were well focused. The beam was neutralized in a charge exchange cell filled with Na vapor. During the first few discharges, the emitter temperature was kept lower than usually, at around 900 °C, and a pure Na beam was produced. When the Na started to be depleted in the ceramic, resulting in a lower beam emission signal, the temperature was raised and in a few discharges both the Li I line as well as the Na I line could be measured, allowing a comparison of the evaluated densities from both signals.

After the positive results (see section 4) of the combined emitter test, filters were purchased (FWHM = 1.5 nm), a Li/Na emitter with Li:Na = 1:9 produced and emission profiles with high spatial and temporal resolution were acquired using the filter-PM-setup.

4. Results

4.1. Emitter Li:Na = 9:1

For some discharges Na I and Li I emission profiles were simultaneously measured. The Li I emission profile is measured by the upper optic and gives a reference electron density (n_e^{ref}). For n_e^{ref} the Na I emission is calculated and then compared with the Na I emission profile measured by the lower optics. Fig. 5 shows the normalized emission profiles modeled with n_e^{ref} as input in comparison with the normalized measured profile. The excellent

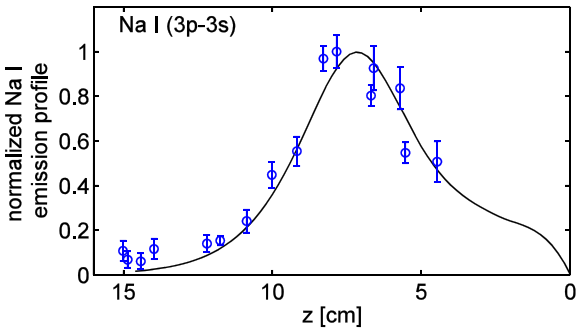

Fig. 5. #21990: modeled emission profile (black) and measured data (blue). (For interpretation of the references to colour in this figure legend, the reader is referred to the web version of this article.)

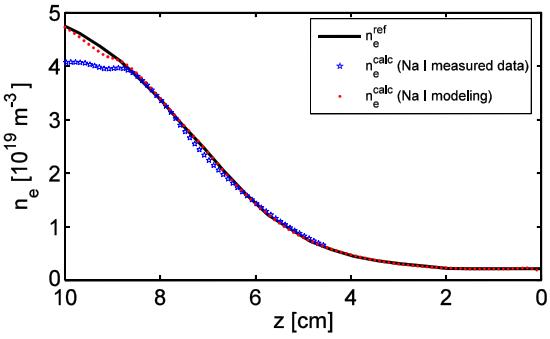

Fig. 6. #21990: n_e^{ref} (black), n_e calculated of Na I measured (blue stars), n_e calculated of Na I modeled (red dots).

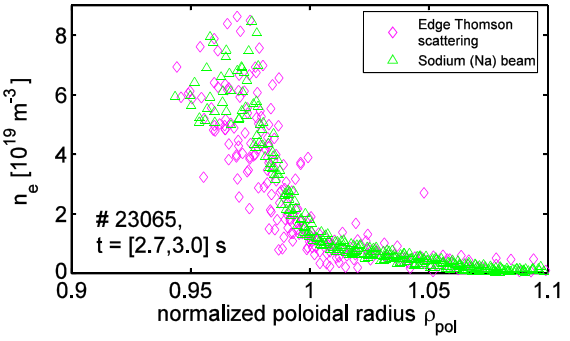

Fig. 7. n_e profiles determined by Na beam diagnostic (green) and Edge Thomson scattering (pink).

agreement of the two profiles proves the validity of the underlying atomic database.

In Fig. 6 the reconstructed n_e profiles from both the measured and the modeled profiles (as shown in Fig. 5) are compared to n_e^{ref}. Within the ETB zone the n_e profiles are very similar.

4.2. Emitter Li:Na = 1:9

In the second, dedicated Na experiment, where the Na I emission was recorded with high spatial and temporal resolution, n_e profiles were reconstructed on all plasma discharges of two experimental days.

As example Fig. 7 shows the n_e profiles derived from the Na beam in comparison with profiles from the edge Thomson scattering diagnostic [10]. The gradient in the ETB zone is well resolved up to the top of the pedestal.

5. Conclusions

In dedicated combined Li/Na emitter experiments it was shown that the atomic database [1] is valid.

The lower lifetime of the Na 3p state leads to a lower occupation number density of this state and results in a larger than expected penetration depth of the Na beam, so that its accessible radial range is comparable to Li at the same acceleration voltages.

The Li beam was successfully replaced by a Na beam for two experimental days. The resulting n_e profiles from Na I emission profiles were of comparable quality as the usual ones from Li I emission. A more detailed evaluation of the measured data on these two days is still ongoing.

In the near future experiments are planned with a pure Na emitter with the aim of (a) exploring the potential of the higher charge exchange cross sections of Na with e.g. He^{2+} or C^{6+} and (b) utilizing the shorter lifetime of the Na 3p state for n_e fluctuation measurements with higher spatial resolution.

Acknowledgements

This work, supported by the European Communities under the Contract of Association between EURATOM and the Austrian Academy of Sciences, was carried out within the framework of the European Fusion Development Agreement. The views and opinions expressed herein do not necessarily reflect those of the European Commission. The mobility programme of the EC has supported participation of J.K. in experiments at IPP Garching.

References

[1] K. Igenbergs et al., At. Data Nucl. (Data Tables in print).
[2] L. Horton et al., Nucl. Fus. 45 (2005) 856.
[3] R. Brandenburg et al., Fus. Technol. 36 (1999) 289.
[4] M. Reich et al., Plasma Phys. Control. Fus. 46 (2004) 797.
[5] E. Wolfrum et al., Rev. Sci. Instrum. 77 (2006) 033507.
[6] R. Fischer et al., Plasma Phys. Control. Fus. 50 (2008) 085009 (26pp).
[7] S. Zoletnik et al., Phys. Plasmas 6 (1999) 4239.
[8] J. Schweinzer et al., Plasma Phys. Control. Fus. 34 (1992) 1173.
[9] J. Neuhauser et al., PPCF 44 (2002) 855.
[10] B. Kurzan et al., Rev. Sci. Instrum. 72 (2001) 1111.